







Article

Influence of Low Sintering Temperature on $\text{BaCe}_{0.2}\text{Zr}_{0.6}\text{Y}_{0.2}\text{O}_{3-\delta}$ IT-SOFC Perovskite Electrolyte Synthesized by Co-Precipitation Method

Muhammad Rafique ^{1,*}, Neelam Safdar ², Muneeb Irshad ³, Muhammad Usman ⁴, Maaz Akhtar ⁵, Muhammad Wajid Saleem ⁶, Muhammad Mujtaba Abbas ^{7,*}, Ahmed Ashour ⁸ and Manzoore Elahi Soudagar ⁹

¹ Department of Physics, University of Sahiwal, Sahiwal 57000, Pakistan

² Department of Physics, University of Gujrat, Gujrat 50700, Pakistan; neelamsafdar800@gmail.com

³ Department of Physics, University of Engineering and Technology, Lahore 54890, Pakistan; muneebirshad@gmail.com

⁴ Department of Mechanical Engineering, University of Engineering and Technology, Lahore 54890, Pakistan; muhammadusman@uet.edu.pk

⁵ Mechanical Engineering Department, NED University of Engineering and Technology, Karachi 75270, Pakistan; maaz@neduet.edu.pk

⁶ Department of Mechanical and Mechatronics Engineering, College of Engineering, Dhofar University, Salalah 211, Oman; msaleem@du.edu.om

⁷ Department of Mechanical Engineering, New Campus, University of Engineering and Technology, Lahore 39021, Pakistan

⁸ Engineering Mathematics and Physics Department, Faculty of Engineering and Technology, Future University in Egypt, New Cairo 11845, Egypt; ahmed.ashour@fue.edu.eg

⁹ Department of Mechanical Engineering and University Centre for Research & Development, Chandigarh University, Mohali 140413, Punjab, India; me.soudagar@gmail.com

* Correspondence: mrafique.uet@gmail.com (M.R.); m.mujtaba@uet.edu.pk (M.M.A.)



Citation: Rafique, M.; Safdar, N.; Irshad, M.; Usman, M.; Akhtar, M.; Saleem, M.W.; Abbas, M.M.; Ashour, A.; Soudagar, M.E. Influence of Low Sintering Temperature on $\text{BaCe}_{0.2}\text{Zr}_{0.6}\text{Y}_{0.2}\text{O}_{3-\delta}$ IT-SOFC Perovskite Electrolyte Synthesized by Co-Precipitation Method. *Materials* **2022**, *15*, 3585. <https://doi.org/10.3390/ma15103585>

Academic Editor: Jose Antonio Alonso

Received: 17 March 2022

Accepted: 11 May 2022

Published: 17 May 2022

Publisher's Note: MDPI stays neutral with regard to jurisdictional claims in published maps and institutional affiliations.



Copyright: © 2022 by the authors. Licensee MDPI, Basel, Switzerland. This article is an open access article distributed under the terms and conditions of the Creative Commons Attribution (CC BY) license (<https://creativecommons.org/licenses/by/4.0/>).

Abstract: $\text{BaCe}_{0.2}\text{Zr}_{0.6}\text{Y}_{0.2}\text{O}_{3-\delta}$ (BCZY) perovskite electrolytes were synthesized for intermediate-temperature solid oxide fuel cell with a cost-effective and versatile co-precipitation method. The synthesized BCZY electrolytes were sintered at 900, 1000, and 1100 °C to observe the effects of low sintering temperature on the structural, morphological, thermal, and electrical properties of BCZY. All BCZY electrolytes materials exhibited a crystalline perovskite structure and were found to be thermally stable. The crystallinity and conductivity of BCZY electrolyte enhanced with increased sintering temperature, due to the grain growth. At the same time, secondary phases of carbonates were also observed for samples sintered at a temperature lower than 1100 °C. The BCZY sintered at 1100 °C exhibited a density >95%, and a power density of 350 mWcm⁻² with open-circuit voltage 1.02 V at 650 °C was observed due its dense and airtight structure. Based on the current investigation, we suggest that the $\text{BaCe}_{0.2}\text{Zr}_{0.6}\text{Y}_{0.2}\text{O}_{3-\delta}$ perovskite electrolyte sintered at a temperature of 1100 °C is a suitable electrolyte for IT-SOFC.

Keywords: BCZY; electrolyte; perovskite; co-precipitation

1. Introduction

Fuel cells have gained a lot of interest during the last decade as an alternative energy resource. Much focus is devoted to making them efficient and cost-effective [1,2]. Solid oxide fuel cells have received much consideration, among others, because of their fuel flexibility, inexpensive catalyst, and efficiency [3,4]. SOFCs have a solid electrolyte between two electrodes: cathode and anode [5–7]. SOFCs operating at high temperatures (at about 1000 °C) give high conductivities (>10⁻¹ Scm⁻¹) and efficiencies, thus limiting their commercial usage [3,8–10]. Therefore, reducing the operating temperature will help with the stability, performance, efficiency, and commercialization of SOFCs [11]. Reducing operating

temperature assists in terms of manufacturing costs, material stability, and operational cost, but resistive losses across the solid electrolyte and overpotential at electrodes cause an increase in operating temperatures. Three approaches are commonly used to reduce these losses: (i) decrease in electrolyte thickness, (ii) usage of materials having high conductivities at low operating temperatures, and (iii) usage of electrodes with low polarization resistance [12–14].

The electrolyte is a key component of SOFCs that greatly affects their performance; therefore, developments in electrolyte materials are crucial in lowering the working temperature of SOFCs with better chemical stability and high ionic conductivity [15–18]. Many ionic conductors, such as ZrO_2 , $LaGaO_3$, YSZ, and CeO_2 , have been investigated as electrolytes in SOFCs. Still, these electrolytes require a high activation energy and temperature to provide maximum conductivity [19]. On the other hand, proton conductors are promising candidates for SOFC electrolytes since they have high protonic conductivity at low temperatures [20,21]. BCZYs from cerate and zirconate families are considered promising perovskite electrolytes because, at low temperatures, they exhibit high proton conductivity [20,22,23]. Ni et al. observed that barium cerate ($BaCeO_3$) electrolytes exhibit high ionic conductivity that can be enhanced to $10^{-2} \Omega^{-1}cm^{-1}$ by (15–20%) doping of yttrium. However, their chemical stability suffered due to the presence of hydrocarbons at the anode site that react with carbon dioxide, resulting in the poor performance of the cell [24]. Barium zirconate ($BaZrO_3$), on the other hand, shows greater stability in a CO_2 atmosphere but exhibits low ionic conductivity [25]. Therefore, composite electrolytes of $BaCeO_3$ and $BaZrO_3$ were developed, exhibiting both high conductivity and chemical stability. It is also reported that BCZY electrolytes-based SOFCs had shown high short-term power densities of about 0.4 and $1.0 Wcm^{-2}$ at 600 and 700 °C [26–28]. Yuqing Meng et al. synthesized $BaCe_{0.7}Zr_{0.1}Y_{0.2-x}Sm_xO_{3-\delta}$ electrolyte materials by using the ball-milling process and sintering at 1400 °C. The reported performance was $410 mWcm^{-2}$ [29]. Another group of researchers also fabricated a BCZY electrolyte with dopants (2 mol% Fe, Ni) and sintered it at 1400 °C. The electrochemical performance obtained was $450 mWcm^{-2}$ [30]. Kang et al. prepared $BaCe_{0.7}Zr_{0.2}Y_{0.2}$ (3 mol% Ni as sintering aid) and sintered it at 1200 °C. The performance obtained was $106 mWcm^{-2}$ [31]. The use of a sintering aid also gained considerable interest for the lowering of the sintering temperature. Recently, Zaheer ud Din et al. sintered $BaCe_{0.7}Zr_{0.1}Y_{0.2}O_{3-\delta}$ (BCZY) perovskite electrolytes at 1150 °C, using sintering aids ($CuO-Bi_2O_3$), and improved the electrochemical performance of a proton-conducting electrolyte that was observed at a previously reported high temperature [32].

The synthesis routes are crucial in attaining the required properties of the material. The same material synthesized with different methods will exhibit a different structure and morphology. The optimization of the sintering temperature for each route is therefore necessary to obtain a material of desired properties and densification. The Co-precipitation synthesis route, among other wet chemical routes, is considered to be a versatile, simple, and cost-effective route to obtain fine and uniformly shaped powder material [12–14,32].

In the current project, the lowest possible sintering temperature was optimized for a BCZY ($BaCe_{0.2}Zr_{0.6}Y_{0.2}O_{3-\delta}$) electrolyte synthesized via a cost-effective co-precipitation method. The upshots of a varying sintering temperature on structural, morphological, electrical, and thermal properties were investigated through different characterizations.

2. Experimental Details

$BaCe_{0.2}Zr_{0.6}Y_{0.2}O_{3-\delta}$ powder electrolyte was synthesized by using Na_2CO_3 as a precipitating agent through one-step co-precipitation. $Y(NO_3)_3 \cdot 6H_2O$ (>99%), $Ba(NO_3)_2$ (>99%), $Ce(NO_3)_3 \cdot 6H_2O$ (>99%), and $Zr(NO_3)_4 \cdot 5H_2O$ (>99%) were used as precursor materials. The nitrate salts were dissolved in deionized water under continuous stirring and heating. A separate sodium carbonate solution (Na_2CO_3) was formed. The molar ratio of sodium carbonate and metal cations was adjusted to 1:1 to precipitate the metal cations. The carbonate solution was added dropwise in nitrate solution, with continuous stirring at 90 °C, and the filtration process collected white precipitates, which were dried at 150 °C for

2 h. The dried powder was then sintered in a vacuum furnace at 900, 1000, and 1100 °C temperatures for 4 h, with at a rate of 3 °C/min. The sintered powder was then grinded and pressed into pellets for analysis.

An X-ray diffractometer analyzed the structural phases and crystallinity of BCZY electrolyte powder. The surface morphology was investigated through SEM (JEOL, JSM 6360). The thermal stability up to 900 °C in air was observed by SETARAM, with a rate of 10 °C/min. The density was measured by using the Archimedeian immersion method. The sides of the pellets were coated with silver paste for measuring ionic conductivity, using the four-point probe DC method.

3. Results

3.1. XRD Analysis

Figure 1 shows the XRD patterns of the synthesized $\text{BaCe}_{0.2}\text{Zr}_{0.6}\text{Y}_{0.2}\text{O}_{3-\delta}$ electrolytes sintered at 900, 1000, and 1100 °C. The XRD patterns represent the diffraction peaks at 30°, 42°, 53°, 63°, and 71°, corresponding to (111), (102), (103), (107), and (220) planes, respectively. These planes indicate the cubic phase of BCZY the composite (JCPDS Nos. 89-2486 and 82-2372).

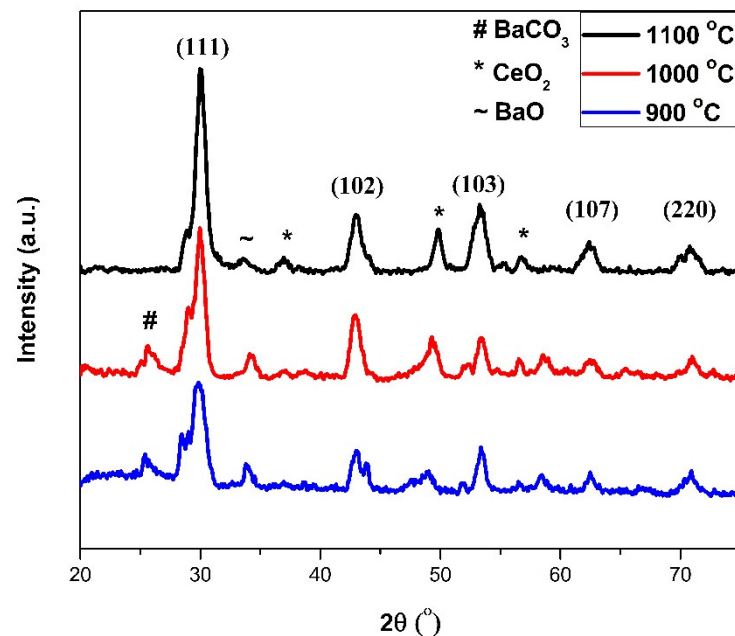


Figure 1. XRD spectra of sintered $\text{BaCe}_{0.2}\text{Zr}_{0.6}\text{Y}_{0.2}\text{O}_{3-\delta}$ electrolyte.

It is clear from the spectra that, with an increased sintering temperature, the shape of the peaks (e.g., reflection (111)) sharpened, depicting increased crystallinity of the samples. The crystallinity increased due to improvement in grain growth with temperature. An increase in the sintering temperature enhanced grain boundary movement, resulting in an increased crystallite size [33].

It is also clear from the spectra that secondary phases of barium carbonate (BaCO_3), ceria (CeO_2), and barium oxide exist in BCZY electrolyte material at a low sintering temperature and decreased with increased temperature. This is because of the decomposition of barium carbonate and barium oxide, which start decomposing above 1000 °C in temperature. It is also reported that it can be decomposed completely above a temperature of 1100 °C [34]. Moreover, it is reported that pure BCZY phases can be achieved at high sintering temperatures, due to the decomposition and evaporation of secondary phases; therefore, a high sintering temperature is recommended to attain a proper phase with increased crystallinity.

The crystallite size of the sintered samples was calculated by using Scherrer's equation [35]:

$$L = \frac{K\lambda}{\beta \cos \theta} \quad (1)$$

The calculated average crystallites size was 10.48, 12.681, and 18.51 nm for 900, 1000, and 1100 °C, respectively. The increased crystallite size is because of the fact that boundaries of grain migrated more quickly with the increased sintering temperature.

3.2. Density Measurements

The density of the sintered $\text{BaCe}_{0.2}\text{Zr}_{0.6}\text{Y}_{0.2}\text{O}_{3-\delta}$ electrolytes was measured by using the XRD parameters and Archimedes method. The BCZY has a theoretical density of 6.18 gcm^{-3} . The experimental density was calculated by using the Archimedes principle, using equation [36]:

$$D = W_1 \rho / W_1 - W_2 \quad (2)$$

where ρ is the density of water used as fluid (water at 25 °C is 0.997 gcm^{-3}), W_1 is the weight of the sample in air, and W_2 is the wet weight (in water) [37]. The average relative density was 83%, 90%, and 95% for electrolytes sintered at 900, 1000, and 1100 °C, respectively. The sample sintered at 900, 1000, and 1100 °C showed 17%, 10%, and 5% porosity, respectively. Hence, the sample sintered at 1100 °C exhibited a dense structure, limiting the leakage of the ions and, thus, making it an efficient electrolyte.

3.3. Surface Morphology

Figure 2 shows the micrographs of sintered $\text{BaCe}_{0.2}\text{Zr}_{0.6}\text{Y}_{0.2}\text{O}_{3-\delta}$ electrolytes. The SEM micrographs clearly show that the surface morphology of BCZY changed with an increased sintering temperature. It can also be observed that pores disappeared with the increased temperature because of diffusion kinetics (mass transport at higher sintering for increase of further bond area and mechanical strength) and recrystallization, which resulted in increased grain size and decreased grain boundaries [38]. Furthermore, the porosity reduced gradually with the rise in temperature, as confirmed by the Archimedes' principle, too. Large-sized grains with dense and compact structures can be observed for materials sintered at 1100 °C in Figure 2c, fulfilling the main requirement of SOFC electrolyte: the electrolyte should be free of pores to prevent diffusion of gases from one side to the other side of the electrolyte.

3.4. Thermal Stability Analysis

The TGA curves in Figure 3 give the temperature-dependent weight loss of sintered $\text{BaCe}_{0.2}\text{Zr}_{0.6}\text{Y}_{0.2}\text{O}_{3-\delta}$ electrolytes. It is clear from the plot that a very small weight loss occurred because the analysis was performed after the sintering, which already evaporated and decomposed the water, nitrate, or organic compounds present within the synthesized materials. Similar behavior was also reported by a group of researchers earlier [39]. The TGA curve in each sample can be categorized into two regions: (i) 30 to 160 °C and (ii) 160 to 900 °C. In Region I (30 to 160 °C), a very small loss occurred due to the evaporation and decomposition of absorbed water in the $\text{BaCe}_{0.2}\text{Zr}_{0.6}\text{Y}_{0.2}\text{O}_{3-\delta}$ electrolytes from the moisture of the ambient environment [40]. In Region II (160 to 900 °C), there was no weight loss observed under heating, thus suggesting that no volatilization or decomposition reactions occurred between 160 and 900 °C; therefore, it will remain chemically stable at the SOFC operating temperature.

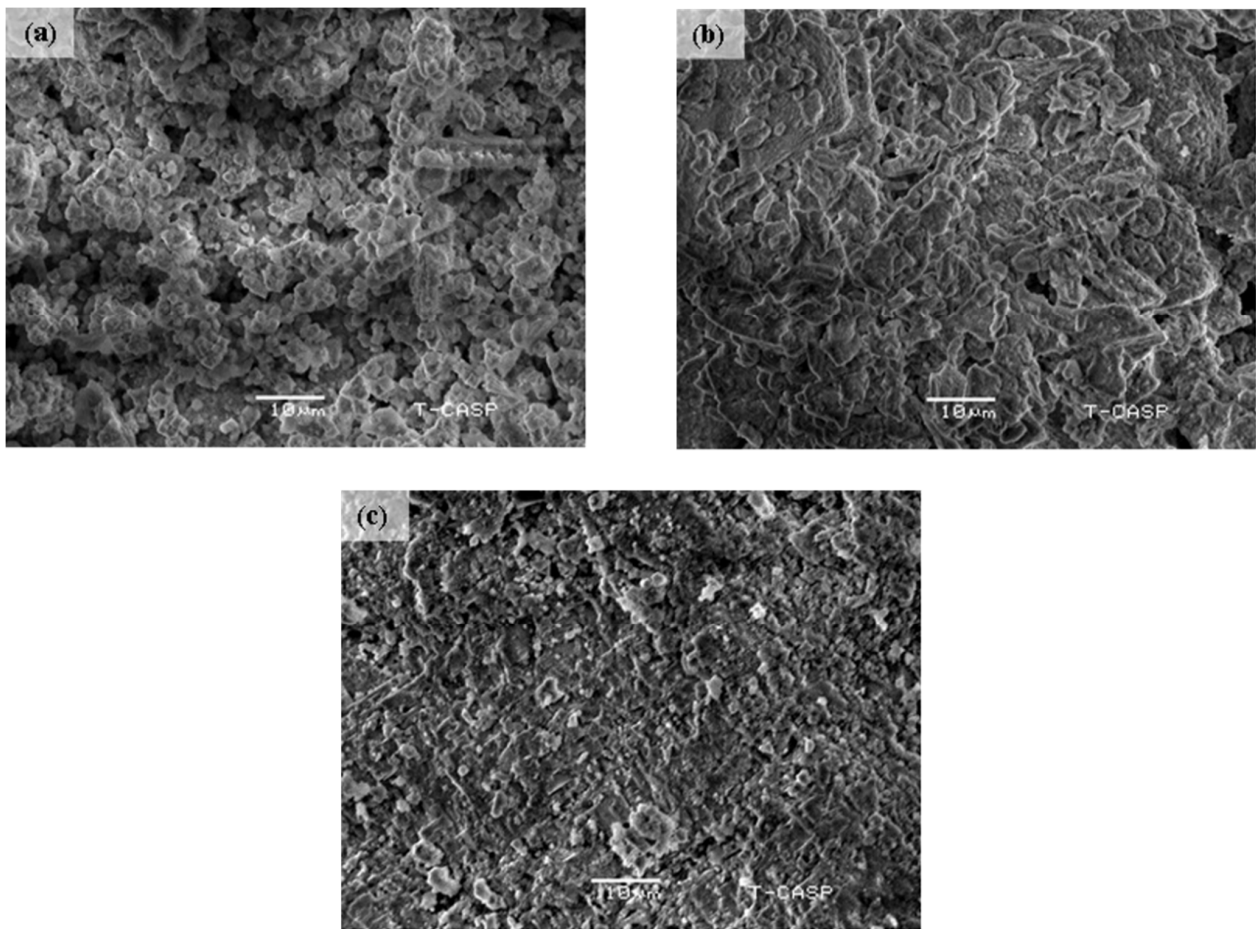


Figure 2. Micrographs of sintered BaCe_{0.2}Zr_{0.6}Y_{0.2}O_{3-δ} electrolyte: (a) 900 °C, (b) 1000 °C, and (c) 1100 °C.

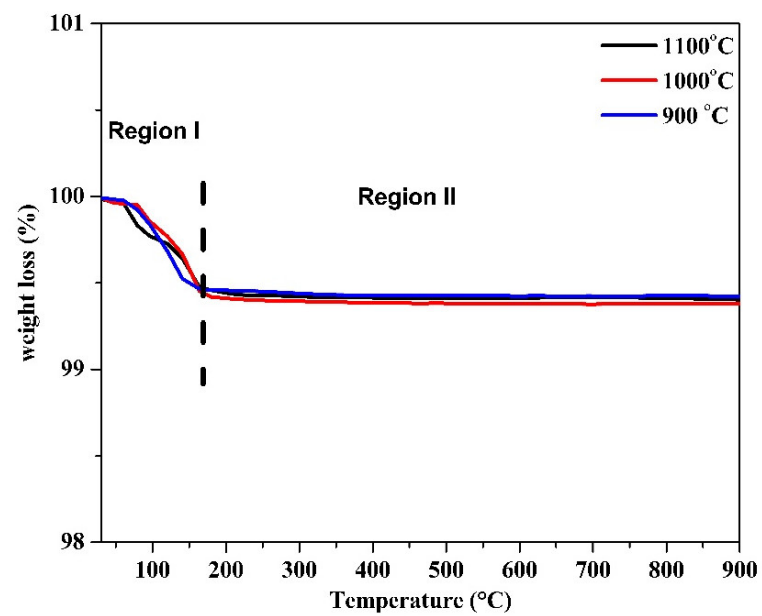


Figure 3. TGA curves for sintered BaCe_{0.2}Zr_{0.6}Y_{0.2}O_{3-δ} electrolyte.

3.5. Conductivity

The measured ionic conductivity of the synthesized BCZY electrolytes is shown in the Arrhenius plot in Figure 4. It was calculated by using the Arrhenius relation [39]:

$$\alpha = \frac{\alpha_0}{T} \exp \frac{E_a}{KT} \quad (3)$$

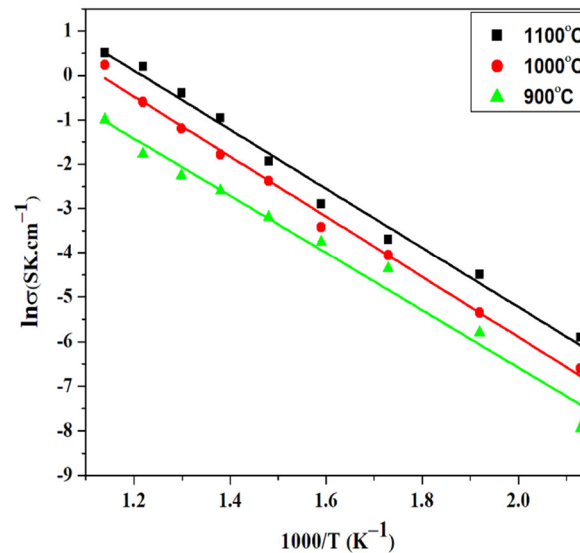


Figure 4. Conductivity curves of sintered $\text{BaCe}_{0.2}\text{Zr}_{0.6}\text{Y}_{0.2}\text{O}_{3-\delta}$ electrolyte.

Figure 4 depicts that conductivity increased as the sintering rose from 900 to 1100 °C. This increased conductivity is because of improved grain growth and microstructural changes. The densification and reduction of pores enhanced the rate of the ions' diffusion through the grain boundaries. Moreover, the secondary phases were minimized due to the increase in temperature, which reduced the electrolyte loses and gas inter-diffusion, resulting in increased conductivity [41]. The activation energy of 0.53 eV was obtained for the electrolyte sintered at 1100 °C. Emiliana et al. reported an activation energy of 0.66–0.68 eV for Y and Pr doped barium zirconate sintered at 1500 °C [42]. Nur syafkeena et al. reported an activation energy of 0.79 eV for the $\text{BaCe}_{0.54}\text{Zr}_{0.36}\text{Y}_{0.1}\text{O}_{3-\delta}$ electrolyte sintered at 1500 °C [43]. However, low activation energy (0.41 eV) for BCZY ($\text{BaCe}_{0.7}\text{Zr}_{0.1}\text{Y}_{0.2}\text{O}_{3-\delta}$) sintered at 1150 °C was also reported when $\text{CuO-Bi}_2\text{O}_3$ (2 mol%) was used as a sintering aid [32].

3.6. Cell Performance

The electrochemical performance of a single cell consisting of Ni-BCZY/BCZY (sintered at 1100 °C)/BCZY-LSCF was evaluated in a 3% H_2 atmosphere at 650 °C and is shown in Figure 5. The $\text{BaCe}_{0.2}\text{Zr}_{0.6}\text{Y}_{0.2}\text{O}_{3-\delta}$ perovskite electrolyte material sintered at 1100 °C was used as an electrolyte, due to its high density and conductivity value. Moreover, it was observed in XRD that the barium carbonate phase decomposed at this temperature; therefore, it is more suited for the electrochemical evaluations among all samples. The maximum power density obtained was 350 mW/cm^2 , with an OCV of 1.02 V. The measured performance of the BCZY electrolyte sintered at 1100 °C is comparable to the electrolytes sintered at high temperatures [44,45].

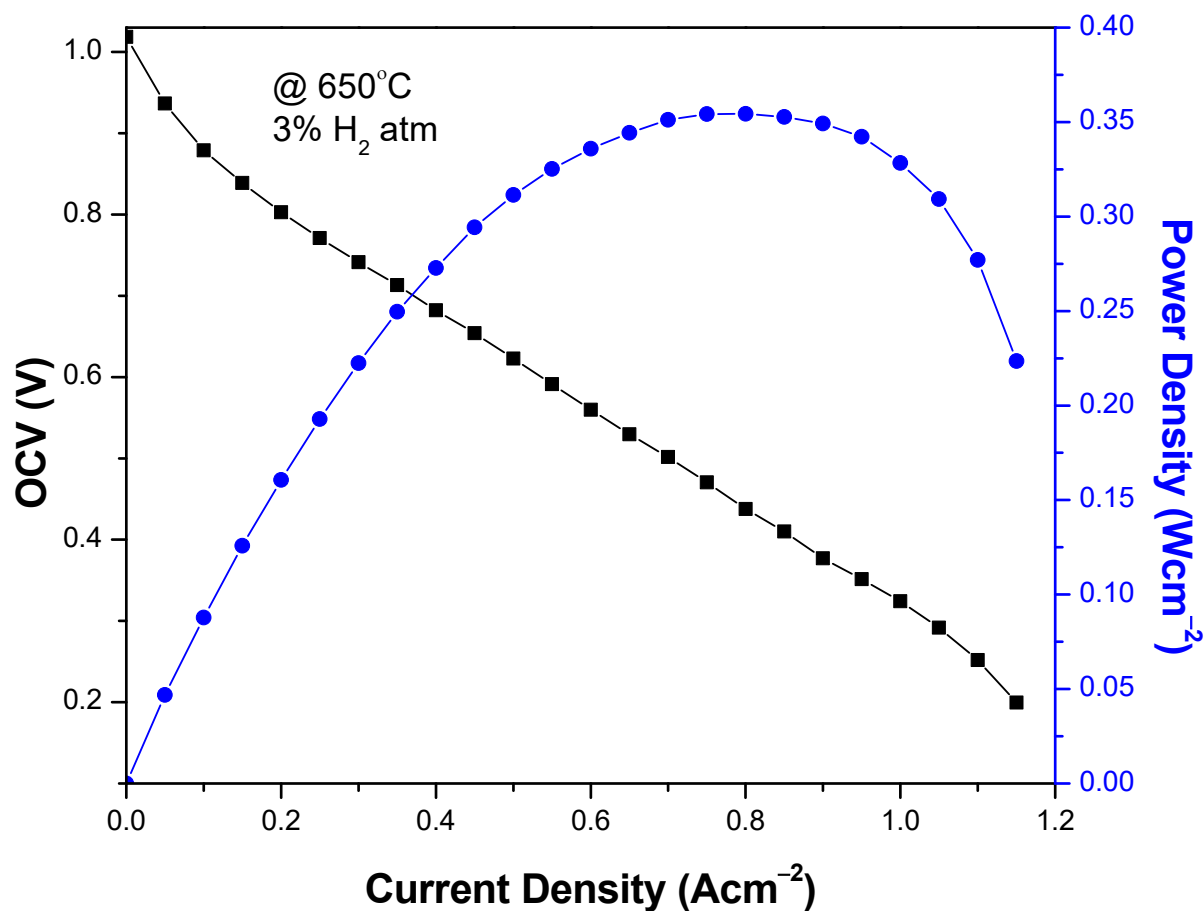


Figure 5. Electrochemical performance of cell with $\text{BaCe}_{0.2}\text{Zr}_{0.6}\text{Y}_{0.2}\text{O}_{3-\delta}$ electrolyte sintered at $1100\text{ }^{\circ}\text{C}$.

The performance can be enhanced by increasing the sintering temperature up to $1300\text{ }^{\circ}\text{C}$, which is still lower compared to the reported temperatures. The secondary phases will be removed by the high sintering temperature, and, therefore, single-phase BCZY will give a better electrochemical performance. A comparative table for the performance of the SOFC with the BCZY electrolyte is given in Table 1.

Table 1. Power Densities of SOFC with different compositions of BCZY electrolyte [46].

Electrolyte	$\text{BaCe}_{0.4}\text{Zr}_{0.4}\text{Y}_{0.2}\text{O}_{3-\delta}$	$\text{BaCe}_{0.5}\text{Zr}_{0.35}\text{Y}_{0.15}\text{O}_{3-\delta}$	$\text{BaZr}_{0.4}\text{Ce}_{0.4}\text{Y}_{0.2}\text{O}_{3-\delta}$	$\text{BaZr}_{0.1}\text{Ce}_{0.7}\text{Y}_{0.2}\text{O}_{3-\delta}$
Cathode	PrNi	LSC	BSCF	LSCF
Anode	Ni-BCZY	Ni-BCZY	Ni-BCZY	Ni-BCZY
Temperature ($^{\circ}\text{C}$)	550	550	600	600
Power Density (mW cm^{-2})	63	300	360	477

4. Discussion

The structural analysis (Figure 1) confirmed the cubic phase of $\text{BaCe}_{0.2}\text{Zr}_{0.6}\text{Y}_{0.2}\text{O}_{3-\delta}$ (BCZY) perovskite electrolytes (JCPDS Nos. 89-2486 and 82-2372). The structural analysis also showed increased crystallinity of the samples with increasing sintering temperature, because of enhanced grain growth at high temperatures. The calculated average crystal-

lites size was 10.48, 12.681, and 18.51 nm for $\text{BaCe}_{0.2}\text{Zr}_{0.6}\text{Y}_{0.2}\text{O}_{3-\delta}$ perovskite electrolytes sintered at 900, 1000, and 1100 °C, respectively. The increase in sintering temperature caused better grain boundary movement because grain boundaries migrate more quickly with increased temperature, resulting in increased crystallite size. Secondary planes of barium carbonate (BaCO_3), ceria (CeO_2), and barium oxide (BaO) are also observed in $\text{BaCe}_{0.2}\text{Zr}_{0.6}\text{Y}_{0.2}\text{O}_{3-\delta}$ electrolytes. The intensity of these secondary planes decreased with increased temperature. The decomposition of barium carbonate and barium oxide starts above 1000 °C temperature, and it is also reported that it decomposes completely at a temperature >1100 °C.

The density of the synthesized $\text{BaCe}_{0.2}\text{Zr}_{0.6}\text{Y}_{0.2}\text{O}_{3-\delta}$ perovskite electrolytes was calculated by the Archimedean principle. The $\text{BaCe}_{0.2}\text{Zr}_{0.6}\text{Y}_{0.2}\text{O}_{3-\delta}$ electrolytes sintered at 900, 1000, and 1100 °C showed 17%, 10%, and 5% porosity, respectively, depicting that $\text{BaCe}_{0.2}\text{Zr}_{0.6}\text{Y}_{0.2}\text{O}_{3-\delta}$ sintered at 1100 °C exhibited a dense structure, thus limiting the leakage of the ions and making it an efficient electrolyte.

The surface morphology of $\text{BaCe}_{0.2}\text{Zr}_{0.6}\text{Y}_{0.2}\text{O}_{3-\delta}$ perovskite electrolytes revealed that pores disappeared with the increased temperature because of diffusion kinetics and recrystallization. Furthermore, the porosity also reduced gradually with the temperature rise, as confirmed by Archimedes' principle. Large-sized grains with dense and compact structures can be observed for material sintered at 1100 °C in Figure 2c, fulfilling the main requirement of SOFC electrolyte: the electrolyte should be free of pores to prevent diffusion of gases.

Our thermal analysis (Figure 3) showed a small weight loss because it was performed after the sintering, which already evaporated and decomposed the water, nitrate, or organic compounds present in $\text{BaCe}_{0.2}\text{Zr}_{0.6}\text{Y}_{0.2}\text{O}_{3-\delta}$ perovskite electrolytes. The weight loss occurred only from 30 to 160 °C because of evaporation and decomposition of absorbed water present in $\text{BaCe}_{0.2}\text{Zr}_{0.6}\text{Y}_{0.2}\text{O}_{3-\delta}$. The presence of a small amount of water was attributed to the moisture of the ambient environment. It can be inferred that sintered $\text{BaCe}_{0.2}\text{Zr}_{0.6}\text{Y}_{0.2}\text{O}_{3-\delta}$ electrolytes remained chemically stable from room temperature to 900 °C.

Figure 4 depicts that, with an increased sintering temperature (900 to 1100 °C), the conductivity of $\text{BaCe}_{0.2}\text{Zr}_{0.6}\text{Y}_{0.2}\text{O}_{3-\delta}$ perovskite electrolytes increased. This increased conductivity is because of improved grain growth and microstructural changes. The densification and reduction of pores enhanced the rate of ions diffusion through grain boundaries. Moreover, secondary phases were minimized due to the increase in temperature, which reduced the electrolyte losses and gas inter-diffusion, resulting in increased conductivity. The highest conductivity was observed for the $\text{BaCe}_{0.2}\text{Zr}_{0.6}\text{Y}_{0.2}\text{O}_{3-\delta}$ electrolyte sintered at 1100 °C, having an activation energy of 0.53 eV. Figure 5 shows the electrochemical performance of the button cell comprising Ni-BCZY/BCZY (sintered at 1100 °C)/BCZY-LSCF. The $\text{BaCe}_{0.2}\text{Zr}_{0.6}\text{Y}_{0.2}\text{O}_{3-\delta}$ electrolyte sintered at 1100 °C is used as an electrolyte due to its high density and conductivity value. The power density obtained was 350 mW/cm² with OCV of 1.02V at 650 °C, suggesting that the $\text{BaCe}_{0.2}\text{Zr}_{0.6}\text{Y}_{0.2}\text{O}_{3-\delta}$ electrolyte sintered at 1100 °C can be utilized as SOFC. However, a high performance can be yielded if the sintering temperature of the $\text{BaCe}_{0.2}\text{Zr}_{0.6}\text{Y}_{0.2}\text{O}_{3-\delta}$ composition synthesized by co-precipitation is increased up to 1300 °C.

5. Conclusions

The perovskite BCZY ($\text{BaCe}_{0.2}\text{Zr}_{0.6}\text{Y}_{0.2}\text{O}_{3-\delta}$) electrolyte powder was successfully synthesized by using the co-precipitation method. The temperature was kept at 90 °C during the synthesis, and the synthesis was completed in under two hours. The prepared electrolyte was then sintered at 900, 1000, and 1100 °C to enhance the structural, morphological, electrical, and thermal properties. BCZY exhibited the crystallite structure, and the crystallite size increased from 10.48 to 18.51 nm with the increased sintering temperature. Secondary phases (e.g., BaCO_3) were minimized with increased temperature because of their decomposition at high temperatures; therefore, higher than 1100 °C is required for

better performance. SEM micrographs depicted that the porosity decreased, and the structure became denser by raising the temperature from 900 to 1100 °C, because of increased diffusion kinetics, resulting in increased grain size. Furthermore, BCZY exhibited thermal stability as an electrolyte from 160 to 900 °C. The conductivity of BCZY increased with the sintering temperature because of grain growth and densification, which avoided the gas cross-diffusion. A power density of 350 mW/cm² was obtained for the cell that had a BCZY electrolyte sintered at 1100 °C. It can be deduced that the composition BaCe_{0.2}Zr_{0.6}Y_{0.2}O_{3-δ} sintered at a temperature of 1100 °C is a potential candidate for IT-SOFC electrolyte material; however, sintering the current composition at a temperature greater than 1100 °C for 4–5 h can significantly enhance the overall cell performance.

Author Contributions: Data curation, M.R.; Formal analysis, M.I. and M.M.A.; Funding acquisition, A.A.; Investigation, N.S.; Methodology, N.S.; Software, M.U.; Writing—original draft, M.R.; Writing—review & editing, N.S., M.I., M.U., M.A., M.W.S., M.M.A., A.A. and M.E.S. All authors have read and agreed to the published version of the manuscript.

Funding: This research received no external funding.

Institutional Review Board Statement: Not applicable.

Informed Consent Statement: Not applicable.

Data Availability Statement: Not applicable.

Conflicts of Interest: The authors have no conflict of interest.

References

1. Andersson, M.; Paradis, H.; Yuan, J.; Sundén, B. Review of catalyst materials and catalytic steam reforming reactions in SOFC anodes. *Int. J. Energy Res.* **2011**, *35*, 1340–1350. [[CrossRef](#)]
2. Abdalla, A.M.; Hossain, S.; Azad, A.T.; Petra PM, I.; Begum, F.; Eriksson, S.G.; Azad, A.K. Nanomaterials for Solid Oxide Fuel Cells: A Review. *Renew. Sustain. Energy Rev.* **2018**, *82*, 353–368. [[CrossRef](#)]
3. Stambouli, A.; Traversa, E. Solid oxide fuel cells (SOFCs): A review of an environmentally clean and efficient source of energy. *Renew. Sustain. Energy Rev.* **2002**, *6*, 433–455. [[CrossRef](#)]
4. Raza, R.; Ahmad, M.A.; Iqbal, J.; Akram, N.; Gao, Z.; Javed, S.; Zhu, B. Ce_{0.8}(SmZr)_{0.2}O₂-Carbonate Nanocomposite Electrolyte for Solid Oxide Fuel Cell. *Int. J. Energy Res.* **2014**, *38*, 524–529. [[CrossRef](#)]
5. Radenahmad, N.; Afif, A.; Petra, P.I.; Rahman, S.M.; Eriksson, S.G.; Azad, A.K. Proton-Conducting Electrolytes for Direct Methanol and Direct Urea Fuel Cells—A State-of-the-Art Review. *Renew. Sustain. Energy Rev.* **2016**, *57*, 1347–1358. [[CrossRef](#)]
6. Afroze, S.; Karim, A.; Cheok, Q.; Eriksson, S.; Azad, A.K. Latest development of double perovskite electrode materials for solid oxide fuel cells: A review. *Front. Energy* **2019**, *13*, 770–797. [[CrossRef](#)]
7. Irshad, M.; Idrees, R.; Siraj, K.; Shakir, I.; Rafique, M.; Ain, Q.U.; Raza, R. Electrochemical evaluation of mixed ionic electronic perovskite cathode LaNi_{1-x}Co_xO_{3-δ} for IT-SOFC synthesized by high temperature decomposition. *Int. J. Hydrogen Energy* **2020**, *46*, 10448–10456. [[CrossRef](#)]
8. Huang, J.; Xie, F.; Wang, C.; Mao, Z. Development of solid oxide fuel cell materials for intermediate-to-low temperature operation. *Int. J. Hydrogen Energy* **2012**, *37*, 877–883. [[CrossRef](#)]
9. Li, J.-H.; Fu, X.-Z.; Luo, J.-L.; Chuang, K.T.; Sanger, A.R. Evaluation of molybdenum carbide as anode catalyst for proton-conducting hydrogen and ethane solid oxide fuel cells. *Electrochem. Commun.* **2012**, *15*, 81–84. [[CrossRef](#)]
10. Zhu, B. Solid oxide fuel cell (SOFC) technical challenges and solutions from nano-aspects. *Int. J. Energy Res.* **2009**, *33*, 1126–1137. [[CrossRef](#)]
11. Liu, T.; Zhang, X.; Wang, X.; Yu, J.; Li, L. A review of zirconia-based solid electrolytes. *Ionics* **2016**, *22*, 2249–2262. [[CrossRef](#)]
12. Leng, Y.; Chan, S.; Jiang, S.; Khor, K. Low-temperature SOFC with thin film GDC electrolyte prepared in situ by solid-state reaction. *Solid State Ion.* **2004**, *170*, 9–15. [[CrossRef](#)]
13. Rafique, M.S.; Nawaz, H.; Tahir, M.B.; Nabi, G.; Khalid, N. Material and method selection for efficient solid oxide fuel cell anode: Recent advancements and reviews. *Int. J. Energy Res.* **2019**, *43*, 2423–2446. [[CrossRef](#)]
14. Irshad, M.; Siraj, K.; Raza, R.; Rafique, M.; Usman, M.; Ain, Q.U.; Ghaffar, A. Evaluation of densification effects on the properties of 8 mol% yttria stabilized zirconia electrolyte synthesized by cost effective coprecipitation route. *Ceram. Int.* **2020**, *47*, 2857–2863. [[CrossRef](#)]
15. Vijay, P.; Tadó, M.O.; Shao, Z. Statistical method-based calibration and validation of a solid oxide fuel cell model. *Int. J. Energy Res.* **2019**, *43*, 2478–2500. [[CrossRef](#)]
16. Fan, L.; He, C.; Zhu, B. Role of carbonate phase in ceria-carbonate composite for low temperature solid oxide fuel cells: A review. *Int. J. Energy Res.* **2017**, *41*, 465–481. [[CrossRef](#)]

17. Hossain, S.; Abdalla, A.M.; Jamain, S.N.B.; Zaini, J.; Azad, A. A review on proton conducting electrolytes for clean energy and intermediate temperature-solid oxide fuel cells. *Renew. Sustain. Energy Rev.* **2017**, *79*, 750–764. [[CrossRef](#)]
18. Irshad, M.; Khalid, M.; Rafique, M.; Ahmad, N.; Siraj, K.; Raza, R.; Sadiq, M.; Ahsan, M.; Ghaffar, A.; Ashfaq, A. Evaluation of $\text{BaCo}_{0.4}\text{Fe}_{0.4}\text{Zr}_{0.2-x}\text{Ni}_x\text{O}_{3-\delta}$ perovskite cathode using nickel as a sintering aid for IT-SOFC. *RSC Adv.* **2021**, *11*, 14475. [[CrossRef](#)]
19. Irshad, M.; Siraj, K.; Raza, R.; Ali, A.; Tiwari, P.; Zhu, B.; Rafique, A.; Ali, A.; Ullah, M.K.; Usman, A. A Brief Description of High Temperature Solid Oxide Fuel Cell's Operation, Materials, Design, Fabrication Technologies and Performance. *Appl. Sci.* **2016**, *6*, 75. [[CrossRef](#)]
20. Rashid, N.L.R.M.; Samat, A.A.; Jais, A.A.; Somalu, M.R.; Muchtar, A.; Baharuddin, N.A.; Isahak, W.N.R.W. Review on zirconate-cerate-based electrolytes for proton-conducting solid oxide fuel cell. *Ceram. Int.* **2019**, *45*, 6605–6615. [[CrossRef](#)]
21. Zuo, C.; Zha, S.; Liu, M.; Hatano, M.; Uchiyama, M. $\text{Ba}(\text{Zr}_{0.1}\text{Ce}_{0.7}\text{Y}_{0.2})\text{O}_{3-\delta}$ as an Electrolyte for Low-Temperature Solid-Oxide Fuel Cells. *Adv. Mater.* **2006**, *18*, 3318–3320. [[CrossRef](#)]
22. Shimada, H.; Yamaguchi, T.; Sumi, H.; Yamaguchi, Y.; Nomura, K.; Fujishiro, Y. Effect of Ni Diffusion into $\text{BaZr}_{0.1}\text{Ce}_{0.7}\text{Y}_{0.1}\text{Yb}_{0.1}\text{O}_{3-\delta}$ Electrolyte During High Temperature Co-Sintering in Anode-Supported Solid Oxide Fuel Cells. *Ceram. Int.* **2018**, *44*, 3134–3140. [[CrossRef](#)]
23. Zheng, K.; Shen, S. The microstructure effect on ion conduction in composite electrolyte. *Int. J. Energy Res.* **2018**, *42*, 4229–4234. [[CrossRef](#)]
24. Ni, M.; Leung, M.; Leung, D.Y. Technological development of hydrogen production by solid oxide electrolyzer cell (SOEC). *Int. J. Hydrogen Energy* **2008**, *33*, 2337–2354. [[CrossRef](#)]
25. Park, M.Y.; Seo, K.D.; Park, J.-Y.; Lim, H.-T. Durability tests of BCY-BZY electrolyte fuel cells under severe operating conditions. *J. Alloys Compd.* **2018**, *735*, 2341–2347. [[CrossRef](#)]
26. Lyagaeva, J.; Medvedev, D.; Pikalova, E.; Plaksin, S.; Brouzgou, A.; Demin, A.; Tsiakaras, P. A Detailed Analysis of Thermal and Chemical Compatibility of Cathode Materials Suitable for $\text{BaCe}_{0.8}\text{Y}_{0.2}\text{O}_{3-\delta}$ and $\text{BaZr}_{0.8}\text{Y}_{0.2}\text{O}_{3-\delta}$ Proton Electrolytes for Solid Oxide Fuel Cell Application. *Int. J. Hydrogen Energy* **2017**, *42*, 1715–1723. [[CrossRef](#)]
27. Ding, H.; Sullivan, N.P.; Ricote, S. Double perovskite $\text{Ba}_2\text{FeMoO}_{6-\delta}$ as fuel electrode for protonic-ceramic membranes. *Solid State Ion.* **2017**, *306*, 97–103. [[CrossRef](#)]
28. Naceur, H.; Megriche, A.; El Maaoui, M. Effect of sintering temperature on microstructure and electrical properties of $\text{Sr}_{1-x}(\text{Na}_{0.5}\text{Bi}_{0.5})_x\text{Bi}_2\text{Nb}_2\text{O}_9$ solid solutions. *J. Adv. Ceram.* **2014**, *3*, 17–30. [[CrossRef](#)]
29. Meng, Y.; Gao, J.; Huang, H.; Zou, M.; Duffy, J.; Tong, J.; Brinkman, K.S. A High-Performance Reversible Protonic Ceramic Electrochemical Cell Based on a Novel Sm-Doped $\text{BaCe}_{0.7}\text{Zr}_{0.1}\text{Y}_{0.2}\text{O}_{3-\delta}$ Electrolyte. *J. Power Sources* **2019**, *439*, 227093. [[CrossRef](#)]
30. Liu, Z.; Chen, M.; Zhou, M.; Cao, D.; Liu, P.; Wang, W.; Liu, M.; Huang, J.; Shao, J.; Liu, J. Multiple Effects of Iron and Nickel Additives on the Properties of Proton Conducting Yttrium-Doped Barium Cerate-Zirconate Electrolytes for High-Performance Solid Oxide Fuel Cells. *ACS Appl. Mater. Interfaces* **2020**, *12*, 50433–50445. [[CrossRef](#)]
31. Lee, K.-R.; Tseng, C.-J.; Jang, S.-C.; Lin, J.-C.; Wang, K.-W.; Chang, J.-K.; Chen, T.-C.; Lee, S.-W. Fabrication of anode-supported thin BCZY electrolyte protonic fuel cells using NiO sintering aid. *Int. J. Hydrogen Energy* **2019**, *44*, 23784–23792. [[CrossRef](#)]
32. Babar, Z.U.D.; Hanif, M.B.; Gao, J.T.; Li, C.J.; Li, C.X. Sintering Behavior of $\text{BaCe}_{0.7}\text{Zr}_{0.1}\text{Y}_{0.2}\text{O}_{3-\delta}$ Electrolyte at 1150 °C with the Utilization of CuO and Bi_2O_3 as Sintering Aids and Its Electrical Performance. *Int. J. Hydrogen Energy* **2022**, *47*, 7403–7414. [[CrossRef](#)]
33. Ahsan, M.; Irshad, M.; Fu, P.F.; Siraj, K.; Raza, R.; Javed, F. The effect of calcination temperature on the properties of Ni-SDC cermet anode. *Ceram. Int.* **2020**, *46*, 2780–2785. [[CrossRef](#)]
34. Konwar, D.; Nguyen NT, Q.; Yoon, H.H. Evaluation of $\text{BaZr}_{0.1}\text{Ce}_{0.7}\text{Y}_{0.2}\text{O}_{3-\delta}$ Electrolyte Prepared by Carbonate Precipitation for a Mixed Ion-Conducting Sofc. *Int. J. Hydrogen Energy* **2015**, *40*, 11651–11658. [[CrossRef](#)]
35. Gao, Z.; Mao, Z.; Wang, C.; Huang, J.; Liu, Z. Composite Electrolyte Based on Nanostructured $\text{Ce}_{0.8}\text{Sm}_{0.2}\text{O}_{1.9}$ (Sdc) for Low-Temperature Solid Oxide Fuel Cells. *Int. J. Energy Res.* **2009**, *33*, 1138–1144. [[CrossRef](#)]
36. He, Y. Heat capacity, thermal conductivity, and thermal expansion of barium titanate-based ceramics. *Thermochim. Acta* **2004**, *419*, 135–141. [[CrossRef](#)]
37. Arabaci, A.; Öksüzömer, F. Preparation and characterization of 10 mol% Gd doped CeO_2 (GDC) electrolyte for SOFC applications. *Ceram. Int.* **2012**, *38*, 6509–6515. [[CrossRef](#)]
38. Bhuiyan, M.A.; Hoque, S.M.; Choudhury, S. Effects of Sintering Temperature on Microstructure and Magnetic Properties of NiFe_2O_4 Prepared from Nano Size Powder of NiO and Fe_2O_3 . *J. Bangladesh Acad. Sci.* **2010**, *34*, 189–195. [[CrossRef](#)]
39. Irshad, M.; Ain, Q.; Siraj, K.; Raza, R.; Tabish, A.N.; Rafique, M.; Idrees, R.; Khan, F.; Majeed, S.; Ahsan, M. Evaluation of $\text{BaZr}_{0.8}\text{X}_{0.2}$ (X = Y, Gd, Sm) proton conducting electrolytes sintered at low temperature for IT-SOFC synthesized by cost effective combustion method. *J. Alloys Compd.* **2020**, *815*, 152389. [[CrossRef](#)]
40. Irshad, M.; Siraj, K.; Raza, R.; Javed, F.; Ahsan, M.; Shakir, I.; Rafique, M.S. High performance of SDC and GDC core shell type composite electrolytes using methane as a fuel for low temperature SOFC. *AIP Adv.* **2016**, *6*, 025202. [[CrossRef](#)]
41. Chourashiya, M.G.; Patil, J.Y.; Pawar, S.H.; Jadhav, L.D. Studies on Structural, Morphological and Electrical Properties of $\text{Ce}_{1-x}\text{Gd}_x\text{O}_{2-(x/2)}$. *Mater. Chem. Phys.* **2008**, *109*, 39–44. [[CrossRef](#)]
42. Fabbri, E.; Bi, L.; Tanaka, H.; Pergolesi, D.; Traversa, E. Chemically Stable Pr and Y Co-Doped Barium Zirconate Electrolytes with High Proton Conductivity for Intermediate-Temperature Solid Oxide Fuel Cells. *Adv. Funct. Mater.* **2011**, *21*, 158–166. [[CrossRef](#)]

43. Affandi, N.S.M.; Osman, N.; Hassan, O.H. Ac Conductivity of $\text{BaCe}_{0.54}\text{Zr}_{0.36}\text{Y}_{0.1}\text{O}_{3-\delta}$ Electrolyte in Dry and Wet Nitrogen Atmospheres. *AIP Conf. Proc.* **2018**, *2031*, 020018.
44. Ricote, S.; Caboche, G.; Estournès, C.; Bonanos, N. Synthesis, Sintering, and Electrical Properties of $\text{BaCe}_{0.9-x}\text{Zr}_x\text{Y}_{0.1}\text{O}_{3-\delta}$. *J. Nanomater.* **2008**, *2008*, 1–5. [[CrossRef](#)]
45. Baral, A.K.; Tsur, Y. Sintering Aid (Zno) Effect on Proton Transport in $\text{BaCe}_{0.35}\text{Zr}_{0.5}\text{Y}_{0.15}\text{O}_{3-\delta}$ and Electrode Phenomena Studied by Distribution Function of Relaxation Times. *J. Am. Ceram. Soc.* **2019**, *102*, 239–250. [[CrossRef](#)]
46. Irshad, M.; Khalid, M.; Rafique, M.; Tabish, A.N.; Shakeel, A.; Siraj, K.; Ghaffar, A.; Raza, R.; Ahsan, M.; Ain, Q.T. Electrochemical Investigations of $\text{BaCe}_{0.7-x}\text{Sm}_x\text{Zr}_{0.2}\text{Y}_{0.1}\text{O}_{3-\delta}$ Sintered at a Low Sintering Temperature as a Perovskite Electrolyte for It-Sofcs. *Sustainability* **2021**, *13*, 12595. [[CrossRef](#)]